PERGAMON

Aerosol Science 32 (2001) 165–185

Journal of
Aerosol Science

www.elsevier.com/locate/jaerosci

Analysis of growth of non-spherical silica particles in a counterflow diffusion flame considering chemical reactions, coagulation and coalescence

B.W. Lee[1], J.I. Jeong, J.Y. Hwang[1], M. Choi*,[1], S.H. Chung

School of Mechanical and Aerospace Engineering, Seoul National University, San 56-1, Shinlim-dong, Kwanak-ku, Seoul, 151-742, South Korea

Received 14 February 2000; accepted 3 May 2000

Abstract

The evolution of non-spherical silica particles in a counterflow diffusion flame has been studied considering the effects of convection, diffusion, thermophoresis, chemical reactions, coagulation and coalescence. The counterflow geometry provides a one-dimensional flow field along the stagnation point streamline which greatly simplifies the analysis of non-spherical particle growth. Flame analysis of multi-step chemical reactions of hydrogen/oxygen including both oxidation and hydrolysis of $SiCl_4$ has been done to predict flame temperatures, concentrations of gas species and particle generation. The present prediction of flame temperatures was in good agreement with the previous experimental data. Two-dimensional aerosol dynamics in which both particle volume and surface area are independent variables has been then analyzed to obtain the evolution of non-spherical particles which has been compared with the previous experimental data. Several different models of coalescence of silica particles were studied; viscous flow sintering, atomistic diffusion sintering, fast sintering and hybrid sintering models. The use of hybrid sintering model yielded the best agreement with the previous experimental data. Since the collision cross section of non-spherical particles is larger than that of spherical particles having the same volume, coagulation of particles was obviously shown to be enhanced. The important role of axial particle diffusion has been identified in the counterflow diffusion flame. Bi-modal size distributions were obtained at some flame heights.

Keywords: Aggregates; Coalescence; Coagulation

* Corresponding author. Tel.: + 82-2-880-7128; fax: + 82-2-883-0179.

E-mail address: mchoi@plaza.snu.ac.kr (M. Choi).

[1] Also at National CRI Center for Nano Particle Control, Institute of Advanced Machinery and Design, Seoul National University, South Korea.

0021-8502/01/$ - see front matter
PII: S0021-8502(00)00054-9

Nomenclature

$a, \bar{a}$	particle surface area, m^2
a_o	monomer surface area, m^2
c_p	heat capacity, J kg^{-1} K^{-1}
d_{eq}	accessible surface equivalent sphere diameter, m
d_p	primary particle size, m
D_o	pre-exponential term for diffusion, m^2 s^{-1}
$D_{k,l}$	diffusion coefficient of section k, l particles, m^2 s^{-1}
D_p	particle diffusion coefficient (Friedlander, 1977), m^2 s^{-1}
E_{oxi}, E_{hyd}	activation energies for oxidation and hydrolysis of $SiCl_4$, kJ mol^{-1}
E_d	activation energy for diffusion, kJ mol^{-1}
h_i	specific enthalpy of the ith species, J kg^{-1}
$\bar{H}$	inter-sectional sintering coefficient, s^{-1}
k_B	Boltzmann constant, J K^{-1}
$k_{oxi,0}$, $k_{oxi,1}$, $k_{hyd,0}$	pre-exponential factors for oxidation and hydrolysis of $SiCl_4$, s^{-1}, $m^3 mol^{-1} s^{-1}$, $m^3 mol^{-1} s^{-1}$, respectively
m_1, m_2	particle mass, kg
m_k	number of surface area sections of volume k
$n(v, a)$	two-dimensional particle size distribution function, m^{-8}
$n^*(v)$	one-dimensional particle size distribution function, m^{-6}
N_{av}	Avogadro number, mol^{-1}
P	pressure, Pa
P_a	ambient pressure, Pa
r	total number of volume sections
R	ideal gas constant, J mol^{-1}
s_i	surface area accessibility of particle i
T	temperature, K
U	axial component of the velocity, m s^{-1}
U_{ix}	diffusion velocity of the ith species in the x direction, m s^{-1}
U_p	velocity of particle, m s^{-1}
$v, \bar{v}$	particle volume, m^3
v_a	activation volume, m^3 mol^{-1}
v_d	volume of diffusion species, m^3 mol^{-1}
v_o	monomer volume, m^3
V	radial component of the velocity, m s^{-1}
V_k	sectional particle volume density for spherical particles, m^3 m^{-3}
$V_{k,l}$	sectional particle volume density for non-spherical particles, m^3 m^{-3}
W_i	molecular weight of the ith species, kg mol^{-1}
x	axial coordinate, m
$X_{k,l}$	auxiliary parameter used in the sectional approximation
y	radial coordinate, m
Y_i	mass fraction of the ith species
$[i]$	i species concentration, mol m^{-3}

Greek letters	
β	collision frequency function, $m^3\ s^{-1}$
$\bar{\beta}$	inter- and intra-sectional coagulation coefficients, s^{-1}
δ_{k-1}	unit pulse function
$\delta_{v-v_o,a-a_o}$	unit pulse function, m^{-5}
κ	thermophoretic coefficient
ρ	density of the mixture, kg m^{-3}
μ	viscosity of the mixture, Pa s
ν	kinematic viscosity of the mixture, $m^2\ s^{-1}$
λ	thermal diffusivity, W $m^{-1}\ K^{-1}$
Θ	step function
σ	surface tension, J m^{-2}
$\tau_{f,atom}$	characteristic coalescence time for atomistic diffusion mechanism, s
$\tau_{f,vis}$	characteristic coalescence time for viscous flow mechanism, s
$\dot{\omega}_{SiCl_4}$	consumption rate of $SiCl_4$ per unit volume, mol $m^{-3}\ s^{-1}$
$\dot{\omega}_{SiO_2}$	formation rate of SiO_2 per unit volume, mol $m^{-3}\ s^{-1}$

1. Introduction

Flame synthesis can be employed to produce nanoparticles of high purity in large scale. Although extensive studies have been carried out for flame synthesis of various kinds of particles, its fundamentals are not yet well understood since chemical reactions and particle growth occur extremely fast (Pratsinis, 1998; Wooldridge, 1998). Particles are generated by chemical reactions in flames and grow to often form chain-like aggregates and then coalesce to approach spherical shape after passing through high-temperature zone. Burner configurations as well as flow rates and species of fuels and reactants can affect the size and morphology of resulting particles, which ultimately influence the quality of final products such as powders, films or bulk materials.

Extensive studies about the formation and growth of particles in flame have been done. The counterflow diffusion flame burner described by Chung and Katz (1985) has been widely utilized for experimental studies of particle growth in a flame since this burner could produce a flat and stable flame with temperature and species concentrations which are uniform in the horizontal plane. Zachariah, Chin, Semerjian and Katz (1989) studied the growth of silica particles using dynamic light scattering and angular dissymmetry methods in a counterflow diffusion flame reactor. Hung and Katz (1992) measured the variation of particle diameter using dynamic light scattering and discussed the effects of dopants and temperatures in hydrogen–oxygen counterflow diffusion flame. Chung, Tsai and Lin (1991) investigated the effects of flame temperatures and different precursors such as SiH_4 and $SiCl_4$ on particle formation processes in the counterflow diffusion flame. Numerical analysis of aerosol dynamics for particle growth in a counterflow diffusion flame was carried out by Zachariah and Semerjian (1989) using moment and (one-dimensional) sectional methods. They considered the growth of spherical silica particles and utilized measured temperature profiles to calculate flow fields needed for aerosol dynamics calculations. It is noted that non-spherical particles often form as a shape of aggregate composed of

many small primary particles in flame environments and these non-spherical particles may coalesce to become more spherical particles while passing through high-temperature zone. Therefore, it is very important to understand the evolution of non-spherical particle in flames for a proper control of size and morphology of flame generated particles. It is well known that the morphology of flame generated particles is determined by the competition between collision and coalescence of particles (Koch & Friedlander, 1990; Pratsinis, 1998; Windeler, Lehtinen & Friedlander, 1997), for example, faster coalescence than collision would result in spherical particles and on the opposite case, aggregate particles form. Non-spherical silica and titania particles formed at the early stage usually grow and coalesce due to the sintering effect and then become more spherical shape at the later stage (Chang & Biswas, 1992; Cho, Kim & Choi, 1998). Hung and Katz (1992) measured the variation of particle diameters determined from dynamic light scattering which increased at the early stage and then decreased at the later stage due to the effect of coalescence or sintering.

Analyses for non-spherical particle growth can be done by solving two-dimensional aerosol dynamics in which surface area and volume of particles are independent variables. Xiong and Pratsinis (1993) extended the sectional method (Gelbard, Tambour & Seinfeld, 1980) for one-dimensional aerosol dynamics to a two-dimensional aerosol dynamics model using volume and surface area of particles as independent variables and including the effect of coalescence of particles. Simple model accounting for collision and coalescence of particles has been proposed by Kruis, Kusters, Pratsinis and Scarlett (1993) with assuming monodisperse particles. Recently, Okuyama et al. (1998) simulated the growth of non-spherical TiO_2 particles in a thermal CVD reactor using a discrete-sectional method considering two-dimensional representation of particle size distributions and compared simulation results with experimental data. Analyses for non-spherical particle growth in a flame are rarely found except much simplified analyses such as Ehrman, Friedlander and Zachariah (1998) in which flame temperatures were assumed to decrease linearly with distance from the flame, and velocities were evaluated with the assumption of plug flow. Zachariah et al. (1989) analyzed particle growth in a temperature varying flame but they assumed spherical particles.

The objective of the present study is to simulate the growth of non-spherical silica particles generated in a counterflow diffusion flame accounting for multi-step chemical reactions of hydrogen/oxygen diffusion flame coupling with the oxidation and hydrolysis of $SiCl_4$, thermophoresis, particle diffusion, coagulation and coalescence of non-spherical particles. In the present study, temperature and flow fields have been first obtained using flame analysis considering multi-step chemical reactions of hydrogen/oxygen and oxidation/hydrolysis of $SiCl_4$. The growth of non-spherical silica particles have been obtained solving one- and two-dimensional aerosol dynamics with several different sintering models in a counterflow diffusion flame. The results obtained by utilizing various sintering models were compared each other and also with the existing experimental data. The effects of particle diffusion were also investigated and found to be significant in the counterflow diffusion flame for the first time.

2. Analysis

2.1. Combustion analysis with chemical reactions of $SiCl_4$

The counterflow geometry provides a one-dimensional flow field along the stagnation point streamline which greatly simplifies the analysis of particle growth. The basic geometrical

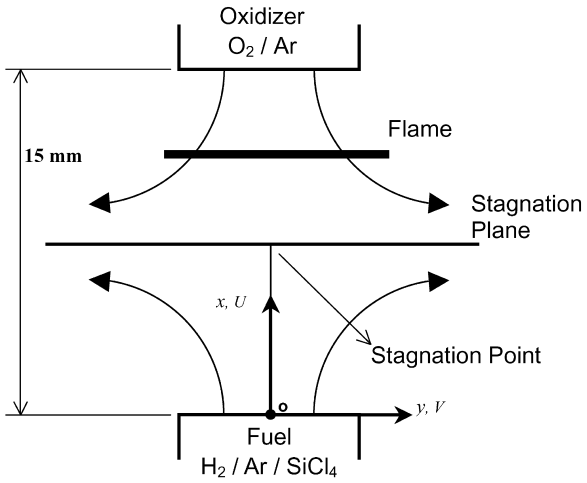

Fig. 1. Schematic diagram of counterflow diffusion flame. The position of particle stagnation would be different from that of flame.

characteristics of the flow field are illustrated in Fig. 1. The oxidant (O_2 diluted with Ar) flows downward and the fuel (H_2 diluted with Ar) flows upward. The two gas streams meet near the middle and flow outward. $SiCl_4$ was used as a precursor of silica particles in the fuel stream. Silica particles are generated by chemical reactions and grow as they flow toward the stagnation plane where they are swept out of the reactor. The flow and temperature fields were calculated following the formulation of Smooke, Puri and Seshadri (1986). The governing equations for mass, momentum, chemical species and energy balances may be written in the following forms when a similarity solution can be assumed for two velocity components; $U = U(x)$, $V = yf(x)$ (Smooke et al., 1986):

Continuity:

$$\rho f + \frac{\mathrm{d}U}{\mathrm{d}x} = 0. \tag{1}$$

Momentum:

$$\rho f^2 + \rho U \frac{\mathrm{d}f}{\mathrm{d}x} + J = \mu \frac{\mathrm{d}^2 f}{\mathrm{d}x^2}, \tag{2}$$

$$\frac{1}{y}\frac{\mathrm{d}P}{\mathrm{d}y} = J = \text{Const.}, \tag{3}$$

$$\frac{\mathrm{d}U}{\mathrm{d}y} = 0. \tag{4}$$

Species:

$$\frac{\mathrm{d}}{\mathrm{d}x}(\rho Y_i U_{ix}) + \rho U \frac{\mathrm{d}Y_i}{\mathrm{d}x} - \dot{\omega}_i W_i = 0. \tag{5}$$

Energy:

$$\frac{\mathrm{d}}{\mathrm{d}x}\left(\lambda\frac{\mathrm{d}T}{\mathrm{d}x}\right)-\rho c_p U\frac{\mathrm{d}T}{\mathrm{d}x}-\sum_{i=1}^{n}\rho Y_i U_{ix} c_p\frac{\mathrm{d}T}{\mathrm{d}x}-\sum_{i=1}^{n}\dot{\omega}_i W_i h_i=0. \tag{6}$$

The chemical model of Maas and Warnatz (1988) containing 8 species and 19 reaction steps was adopted for the analysis of the present hydrogen/oxygen diffusion flame. In the present study, the formation of SiO_2 monomer from the gaseous reactions of $SiCl_4$ has been modeled based on the semi-global approach using rate-determining steps.

For oxidation of $SiCl_4$, two parallel rate-determining steps are (Powers, 1978):

$$\begin{aligned}&SiCl_4 + O_2 \rightarrow SiO_2Cl_3 + Cl,\\ &SiCl_4 \rightarrow SiCl_3 + Cl\end{aligned} \tag{7}$$

and for hydrolysis of $SiCl_4$, the rate-determining step is (Kochubei, 1997)

$$SiCl_4 + H_2O \rightarrow SiOCl_2 + 2HCl. \tag{8}$$

If the forward reaction rates forming SiO_2 from the reactive intermediates produced in reaction (7)–(8) are sufficiently fast, the formation rate of SiO_2, $\dot{\omega}_{SiO_2}$, can be obtained by the following relation using quasi-steady approximation (Powers, 1978; Kochubei, 1997):

$$\begin{aligned}&\dot{\omega}_{SiO_2}\approx\dot{\omega}_{SiCl_4}\approx(\dot{\omega}_{SiCl_{4,oxi}}+\dot{\omega}_{SiCl_{4,hyd}}),\\ &\dot{\omega}_{SiCl_{4,oxi}}=(k_{oxi,0}+k_{oxi,1}[O_2])\exp\left(-\frac{E_{oxi}}{RT}\right)[SiCl_4],\\ &\dot{\omega}_{SiCl_{4,hyd}}=(k_{hyd,0}\exp\left(-\frac{E_{hyd}}{RT}\right)[H_2O][SiCl_4],\end{aligned} \tag{9}$$

Table 1
Parameters used in the simulation

Parameter	Value	Reference
E_{oxi}	402 kJ mol^{-1}	Powers (1978)
$k_{oxi,0}$	1.7×10^{14} s^{-1}	
$k_{oxi,1}$	3.1×10^{13} m^3 mol^{-1} s^{-1}	
E_{hyd}	121.4 ± 2.1 kJ mol^{-1}	Kochubei (1997)
$k_{hyd,0}$	$10^{6.0\pm0.3}$ m^3 mol^{-1} s^{-1}	
D_o	1.1×10^{-6} m^2 s^{-1}	Ehrman (1999)
E_d	328 kJ mol^{-1}	
v_a	-1.92×10^{-5} m^3 mol^{-1}	
v_d	6.9×10^{-6} m^3 mol^{-1}	
σ	0.3 J m^{-2}	

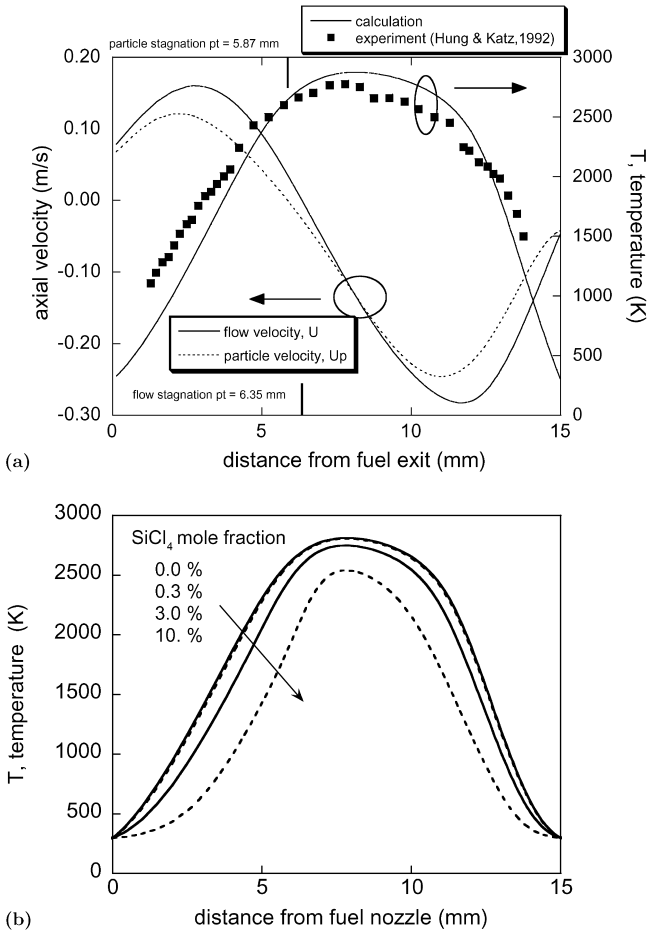

Fig. 2. Velocity and temperature profile: (a) comparison with experimental data ($SiCl_4$ mole fraction: 0.06%) and (b) effects of inlet concentrations.

where $\dot{\omega}_{SiCl_4}$ is the consumption rate of $SiCl_4$ and the pre-exponential factors, $k_{oxi,0}$, $k_{oxi,1}$, $k_{hyd,0}$, are specified in Table 1. The present model implies the first-order dependence of $\dot{\omega}_{SiO_2}$ on $SiCl_4$ concentration.

Fig. 2 shows calculated temperature and velocity profiles. Inlet conditions are listed in Table 2. The calculated temperatures are in good agreement with experiment data (Hung & Katz, 1992). The velocity of particles differs considerably from that of flow due to the thermophoretic effect caused by steep temperature gradients shown in Fig. 2. The estimate of the particle velocity altered by thermophoretic force has been done at each point in the flow field by using the following expression (Talbot, Cheng, Schefer and Willis, 1980):

$$U_p = U|_{flow} - \frac{\kappa v}{T}\frac{dT}{dx}, \tag{10}$$

Table 2
Inlet conditions of fuel and oxidant for counterflow diffusion flame[a]

Fuel stream			Oxidant stream	
H_2	Ar	$SiCl_4$	O_2	Ar
2263 $cm^3\ min^{-1}$	1168 $cm^3\ min^{-1}$	0.06 % (mole fraction)	1818 $cm^3\ min^{-1}$	167 $cm^3\ min^{-1}$

[a]The momentum ratio is 0.8 and the equivalence ratio is 0.62.

where κ thermophoretic coefficient, depends on particle size and could be represented as 0.55 for particles smaller than submicron (Talbot et al., 1980; Nazaroff & Cass, 1987; Kim & Pratsinis, 1988).

The stagnation plane for particles was formed at x equal to 5.87 mm ahead of the flow stagnation point ($x = 6.35$ mm), which would be in agreement with the previous experiment (Hung & Katz, 1992) in which it was reported that the scattering intensity decreased from $x = 5.5$ mm because particles were swept out of the burner at the stagnation plane for particles. The calculations included the effect of chemical reactions of $SiCl_4$ and the case omitting the chemical reactions of $SiCl_4$ also yielded almost the same temperatures due to very low feeding rate of $SiCl_4$ used by Hung and Katz (1992). For larger feeding rates of $SiCl_4$, flame temperatures have been shown to decrease due to larger heat capacity of $SiCl_4$ (see Fig. 2(b)), which is consistent with the results obtained by Allendorf, Bautista and Potkay (1989).

2.2. Analysis of non-spherical particle growth

For particles undergoing generation, diffusion, coagulation and coalescence, two-dimensional aerosol dynamics has been analyzed by solving the following equation (Xiong & Pratsinis, 1993):

$$\frac{\partial}{\partial x}(n(v,a)U_{\mathrm{p}}) - \frac{1}{\tau_{\mathrm{f}}}\frac{\partial}{\partial a}\left(\left[a - \left(\frac{v}{v_{\mathrm{o}}}\right)^{2/3} a_{\mathrm{o}}\right] n(v,a)\right) - \frac{\partial}{\partial x}\left(D_{\mathrm{p}}\frac{\partial n(v,a)}{\partial x}\right)$$

$$= \frac{1}{2}\int_0^v \Theta\left(a > \left(\frac{\bar{v}}{v_{\mathrm{o}}}\right)^{2/3} a_{\mathrm{o}} + \left(\frac{v-\bar{v}}{v_{\mathrm{o}}}\right)^{2/3} a_{\mathrm{o}}\right)$$

$$\times \int_{(\bar{v}/v_{\mathrm{o}})^{2/3} a_{\mathrm{o}}}^{(\bar{v}/v_{\mathrm{o}})a_{\mathrm{o}}} \beta_{\bar{v},v-\bar{v}}(\bar{a}, a-\bar{a}) n(\bar{v},\bar{a}) n(v-\bar{v}, a-\bar{a})\,\mathrm{d}\bar{a}\,\mathrm{d}\bar{v}$$

$$- n(v,a)\int_0^\infty \int_{(\bar{v}/v_{\mathrm{o}})^{2/3} a_{\mathrm{o}}}^{(\bar{v}/v_{\mathrm{o}})a_{\mathrm{o}}} \beta_{v,\bar{v}}(a,\bar{a}) n(\bar{v},\bar{a})\,\mathrm{d}\bar{a}\,\mathrm{d}\bar{v}$$

$$+ N_{av}\dot{\omega}_{\mathrm{SiO_2}}\,\delta_{v-v_{\mathrm{o}},a-a_{\mathrm{o}}}. \tag{11}$$

The first left-hand-side term of the above equation accounts for convection, and the second and the third terms represent coalescence (Koch & Friedlander, 1990) and diffusion of particles, respectively. The first right-hand-side term accounts for the gain of particles with volume v and surface area a by coagulation between smaller particles and the second term accounts for the loss of particles with volume v and surface area a by coagulation with all other particles. Θ is the unit step function which is equal to one when the argument is true, otherwise, zero. The last term accounts for the generation of particles due to chemical reactions.

The collision frequency function, β, depends on the particle size and morphology. In the present study, the description of particle formation and growth is confined in the free-molecular regime. The assumption of free molecular regime could be validated since the resulting maximum mass mean diameter of non-spherical particles in the present calculations is about 0.086 μm and the corresponding Knudsen number is about 22.5.

In the free-molecular regime, β can be written as follows (Xiong & Pratsinis, 1993):

$$\beta = \frac{1}{4}\left(\frac{8k_B T}{\pi m_1} + \frac{8k_B T}{\pi m_2}\right)^{1/2} [(s_1 a_1)^{1/2} + (s_2 a_2)^{1/2}]^2, \tag{12}$$

where s_i, surface area accessibility of particle i, was calculated by the linear interpolation method proposed by Xiong and Pratsinis (1993).

Silica is generally known to coalesce by a viscous flow mechanism and the corresponding characteristic coalescence time, τ_f in Eq. (11), can be obtained from Ehrman et al. (1998) as

$$\tau_{f,vis} = 6.3 \times 10^{-8} d_p \exp\left(\frac{6.1 \times 10^4}{T}\right), \tag{13}$$

where the primary particle diameter, d_p, is obtained by $6v/a$ (Xiong & Pratsinis, 1993; Seto, Shimada & Okuyama, 1995). However, for very small primary particles (less than about 10 nm), the above equation for coalescence rate is known to significantly underestimate the particle growth of silica (Ehrman et al., 1998). The reason might be due to insufficient information about material properties for very small particles less than 10 nm which have different properties from bulk materials (Ehrman, 1999). It seems to be two proposed approaches to compensate the coalescence rate in the initial stage of growth: a fast-sintering model (Ulrich & Subramanian, 1977; Windeler et al., 1997) and an atomistic diffusion sintering model (Ehrman, 1999). For the fast-sintering model, Ulrich and Subramanian (1977) conceived that coalescence might occur almost instantaneously until the particles became large enough (more than 1000 molecules) to exhibit macroscopic viscosity and surface tension. Windeler et al. (1997) also assumed that particles would coalesce rapidly until they grew upto 1000 molecules. Another proposal is to assume atomistic diffusion sintering model (Ehrman, 1999). Recently, Ehrman (1999) assumed that coalescence of silica particles occurred via an atomistic diffusion mechanism and suggested a new coalescence rate including the effect of internal pressure within particles as follows:

$$\tau_{f,atom} = \frac{d_p^3 RT}{128 D_o \sigma v_d} \exp\left[\frac{E_d + v_a(P_a + 4\sigma/d_p)}{RT}\right]. \tag{14}$$

Note that $\tau_{f,atom}$ is proportional to d_p^3 while $\tau_{f,vis}$ is proportional to d_p, therefore, significantly enhanced sintering occurs for very small particles when atomistic diffusion is assumed. In the present study, a hybrid model is also proposed; for small particles, the atomistic diffusion model is used and for large particles, viscous flow sintering model is used since viscous flow sintering mechanism was experimentally proved to be correct for large particles (Seto, Hirota, Fujimoto, Shimada & Okuyama, 1997). In the hybrid model, the smaller characteristic sintering time between $\tau_{f,vis}$ and $\tau_{f,atom}$ was used. Calculations have been done considering viscous flow sintering model, fast sintering model, atomistic diffusion model and hybrid model. The results assuming each model have been compared with the existing experimental data.

2.3. Numerical methods

The two-dimensional particle size domain is divided into a finite number of sections in which the volume distribution, $V_{k,l}$, is assumed to be constant:

$$V_{k,l} = \int_{v_{k-1}}^{v_k} \int_{a_{k,l-1}}^{a_{k,l}} vn(v,a)\,\mathrm{d}a\,\mathrm{d}v, \quad \begin{matrix} k = 1,2,\ldots,r, \\ l = 1,2,\ldots,m_k. \end{matrix} \tag{15}$$

Using a volume-based formulation, the Eq. (11) can be written as follows:

$$\begin{aligned}
\frac{\partial}{\partial x}(U_p V_{k,l}) = {} & \frac{\partial}{\partial x}\left(D_{k,l}\frac{\partial V_{k,l}}{\partial x}\right) + \frac{1}{2}\sum_{i=1}^{k-1}\sum_{j=1}^{k-1}\sum_{s=1}^{m_i}\sum_{t=1}^{m_j}\overline{{}^{1}\beta_{ijk,stl}}V_{i,s}V_{j,t} \\
& + \sum_{i=1}^{k-1}\sum_{s=1}^{m_i}\sum_{t=1}^{l-1}\overline{{}^{2}\beta_{ik,stl}}V_{i,s}V_{k,t} - V_{k,l}\sum_{i=1}^{k-1}\sum_{s=1}^{m_i}\overline{{}^{3}\beta_{ik,sl}}V_{i,s} \\
& + \sum_{i=1}^{k-1}\sum_{s=1}^{m_i}\sum_{t=l+1}^{m_k}\overline{{}^{4}\beta_{ik,stl}}V_{i,s}V_{k,t} + \frac{1}{2}\sum_{s=1}^{l-1}\sum_{t=1}^{l-1}\overline{{}^{5}\beta_{k,stl}}V_{k,s}V_{k,t} \\
& - V_{k,l}\sum_{s=1}^{l-1}\overline{{}^{6}\beta_{k,sl}}V_{k,s} + \sum_{s=1}^{l-1}\sum_{t=l+1}^{m_k}\overline{{}^{7}\beta_{k,stl}}V_{k,s}V_{k,t} \\
& - \frac{1}{2}\overline{{}^{8}\beta_{k,l}}V_{k,l}^2 - V_{k,l}\sum_{s=l+1}^{m_k}\overline{{}^{9}\beta_{k,sl}}V_{k,s} - V_{k,l}\sum_{i=k+1}^{r}\sum_{s=1}^{m_i}\overline{{}^{10}\beta_{ik,sl}} \\
& + \bar{H}_{k,l+1}V_{k,l+1} - \bar{H}_{k,l}V_{k,l} + \delta_{k-1}N_{av}v_o\dot{\omega}_{SiO_2},
\end{aligned} \tag{16}$$

where the inter- and intra-sectional coagulation coefficients, $\bar{\beta}$'s, and sintering coefficients, $\bar{H}$'s, are the same as in Xiong and Pratsinis (1993).

To consider the effect of particle diffusion in two-dimensional aerosol dynamics, diffusion coefficients for non-spherical particles should be defined. Rogak and Flagan (1992) defined the mobility diameter of a non-spherical particle as the diameter of a sphere moving at the same speed as the non-spherical particle and experiencing the same drag force and assumed that the mobility diameter would be proportional to the projected area-equivalent diameter in the free molecular

regime. However, mass fractal dimension was used to calculate the projected area-equivalent diameter (Rogak & Flagan, 1992) while surface fractal dimension was adopted to describe the morphology of non-spherical particles in the present study. Since the drag of non-spherical particle in the free molecular regime would be proportional to the surface area of the particles, an accessible surface area-equivalent sphere diameter (Xiong, Pratsinis & Weimer, 1992), $d_{eq} = \sqrt{s_i a_i/\pi}$, was used to evaluate sectional diffusion coefficient for non-spherical particles as follows:

$$D_{k,l} = \frac{1}{a_o v_o X_{k,l}} \int_{v_{k-1}}^{v_k} \int_{ak,l-1}^{a_{k,l}} D_p(d_{eq})\, da\, dv, \tag{17}$$

where

$$D_p = \frac{k_B T}{3\pi\mu d_{eq}} \left[1 + \frac{2\lambda_g}{d_{eq}} \left(1.257 + 0.4 \exp\left(-\frac{0.55 d_{eq}}{\lambda_g}\right)\right)\right].$$

In principle, the sectional approximation gives more accurate results when number of sections increase for a given size domain, which of course intensifies computational demand. However, in order to alleviate the problems of computing time and memory storage, one can impose a geometric constraint on the section boundaries of the particle volume domain ($v_i = 2v_{i-1}$) (Gelbard et al., 1980; Xiong & Pratsinis, 1993), and employ the number of surface area sections suggested by Xiong and Pratsinis (1993). The total number of sections used in two-dimensional particle space was 861 in the present study. Okuyama et al. (1998) also used the geometric constraint ($v_i = 2v_{i-1}$) for non-spherical particle growth in a thermal CVD reactor and obtained good agreement with experimental data. Simulation using the section spacing factor ($= v_i/v_{i-1}$) of 1.5 was also done and compared with the case using the geometric constraint for spherical particles. The maximum differences of the geometric mean diameter, mass mean diameter and geometric standard deviation were 6.3, 4.5 and 2.5%, respectively. For flame analysis, adaptive grid generation scheme was used (Smooke et al., 1986) to obtain relatively grid independent results. In the present calculations, total number of non-uniform axial grids was 134 and the number of grid points up to the particle stagnation point from the fuel exit was 29. The sensitivity of axial grids for aerosol dynamics was also checked using two different grid systems for non-spherical particle growth; non-uniform grid system with 29 grid points and uniform grid system with 48 grid points between fuel exit and stagnation point of particles. Since the maximum changes of the geometric mean diameter, mass mean diameter and geometric standard deviation were 3.8, 3.0 and 2.7%, respectively, present results were obtained using the non-uniform grid system with 29 grid points between fuel exit and stagnation point of particles.

3. Results and discussion

3.1. The evolution of size distributions in two-dimensional particle space

Fig. 3 shows the evolution of particle size distributions in two-dimensional space, i.e., particle volume and surface fractal dimension, D_s, adopting the viscous flow sintering model (Eq. (13)) without the axial diffusion of particles (Fig. 3(a)) and with the axial diffusion of particles (Fig. 3(b)).

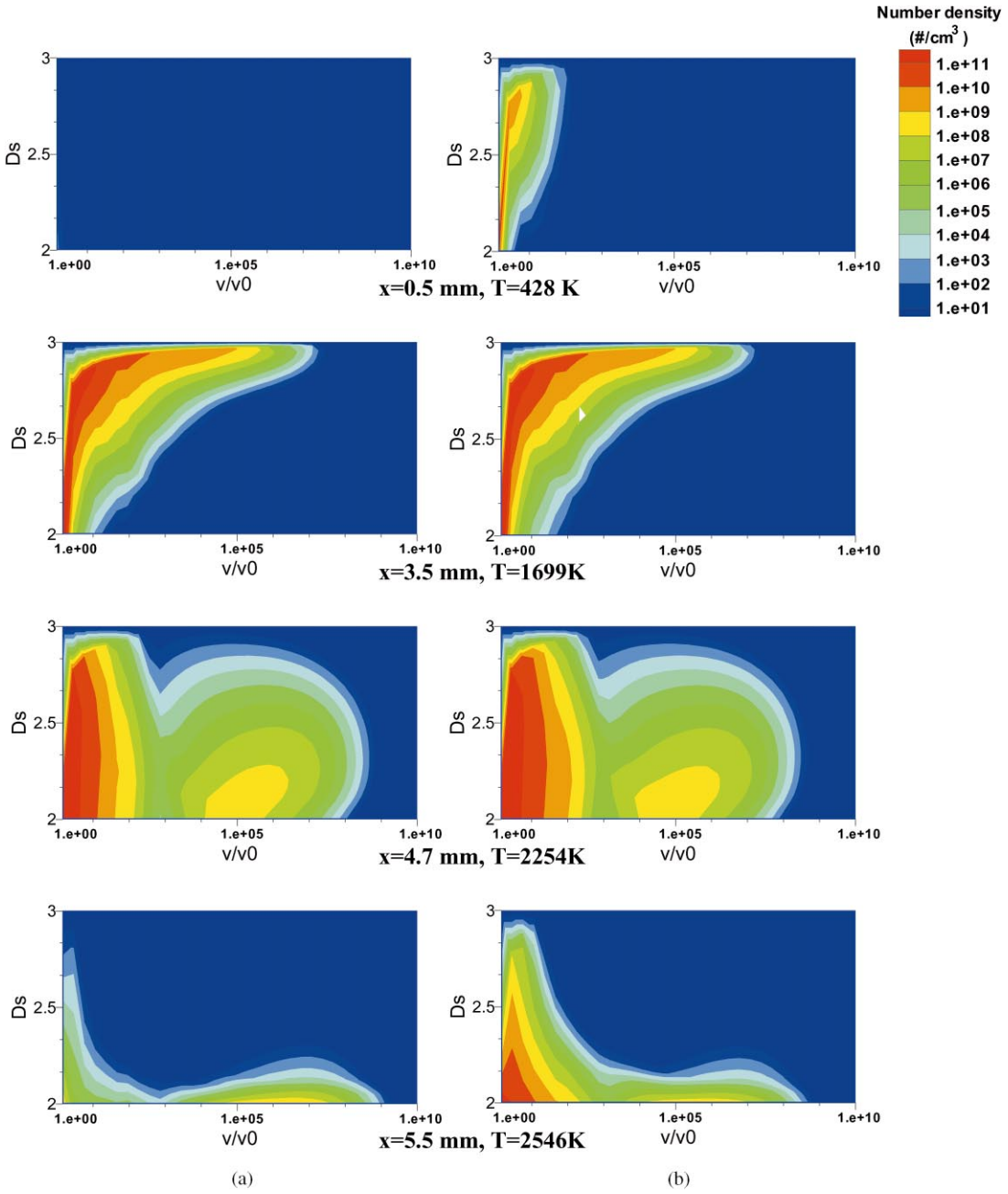

Fig. 3. Evolution of two-dimensional number distributions along the flow stream line: (a) without the axial diffusion of particles, (b) with the axial diffusion of particles using viscous flow sintering model.

The surface fractal dimension, D_s, is defined from the following area–volume relation (Mandelbrot, 1983; Xiong & Pratsinis, 1993):

$$\frac{a}{a_o} = \left(\frac{v}{v_o}\right)^{D_s/3}. \tag{18}$$

For spherical particles, D_s becomes two and for non-spherical particles D_s should be larger than two. For example, in the present two-dimensional representation of particle size distribution (Fig. 3), the bottom lines of $D_s = 2$ in Fig. 3 can be considered as the coalescence lines which correspond to fully coalesced spherical cases and the upper lines of $D_s = 3$ represent the coagulation lines where consisting particles just touch one another upon collision without coalescence. Fig. 3 illustrates how the number density and morphology of particles are changed along the axial direction. Initially formed SiO_2 particles near the burner exit ($x = 0.5$ mm) are spherical particles, i.e. D_s's are close to two even though number is small (Fig. 3(a)) and those particles are coagulated while moving along the axial distance. Near $x = 3.5$ mm, many particles have a high degree of aggregation, i.e. D_s's are close to three. Particle formation process has also taken place to produce many small particle while coagulation process causes particles to have D_s close to three. At $x = 4.7$ mm, particle growth can be seen as well as the effect of coalescence since many particles with high values of D_s at $x = 3.5$ mm are now moving toward the coalescence line. At $x = 5.5$ mm, the effect of coalescence can be seen clearly since most particles now approach to the coalescence line where D_s's are equal to two. In this way, it is clearly shown in Fig. 3(a) how particle generation, coagulation and coalescence affect on the evolution of size distribution in two-dimensional particle space; particle volume and surface fractal. It is also noted that bi-modal size distribution occurs apparently at $x = 4.7$ and 5.5 mm due to the combined effects of chemical reactions and particle coagulation; chemical reactions produce new small particles and finally result in the smaller mode while coagulation of particles contributes to the larger mode. Bi-modal size distributions will be again discussed later.

3.2. The contribution of axial particle diffusion in the counterflow diffusion flame

For modelings of particle growth in flames, the axial diffusion of particles has been usually neglected since convection contribution usually dominates over the particle diffusion (Zachariah & Semerjian, 1989; Ehrman et al., 1998; Xiong & Pratsinis, 1993). However, for nanoparticles, the contribution of axial diffusion may be significant. Especially for the counterflow situation, the existence of flow stagnation plane suggests the small contribution of convection near the stagnation plane and possibly significant contribution of axial particle diffusion. The comparison between Figs. 3(a) and (b) show the effect of particle diffusion. Note that significant difference occurs at $x = 0.5$ and 5.5 mm while small differences are seen at 3.5 and 4.7 mm. The region where the effects of particle diffusion are small coincides with the region where axial flow velocities are relatively high (see Fig. 2(a)) and chemical reactions of $SiCl_4$ occur actively. As shown in Fig. 4, particle formation of SiO_2 is active in the range between $x = 2$ and 5 mm and shows the maximum near $x = 4$ mm. It is also noted in Fig. 4 that hydrolysis dominates at the initial stage while oxidation plays an important role at later stage. In the region, the axial velocities of particles are relatively high compared to the region near the particle stagnation point ($x = 5.87$ mm) and the burner exit

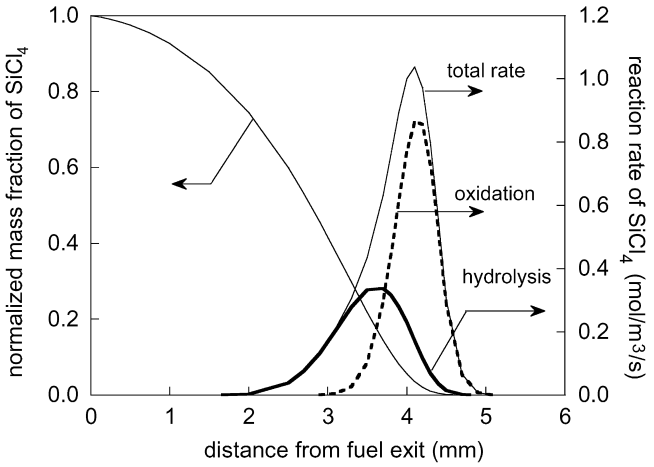

Fig. 4. Contributions of oxidation and hydrolysis of $SiCl_4$ and normalized mass fraction ($Y_i(x)/Y_i(0)$) along the distance from fuel exit.

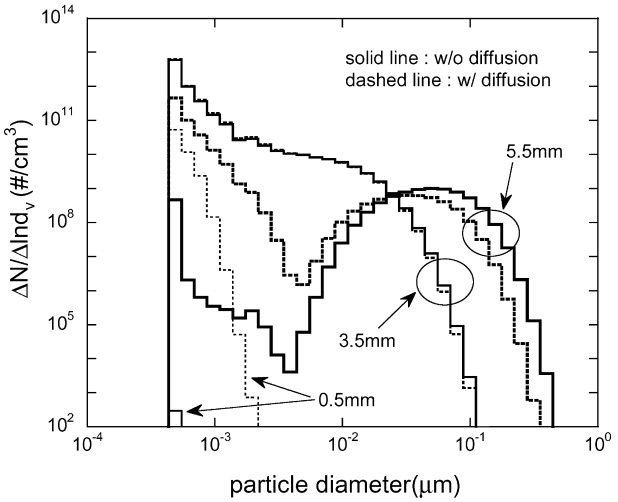

Fig. 5. Effect of particle diffusion on (volume equivalent) number distributions for different axial locations.

(see Fig. 2). Therefore, it is expected that the effects of particle generation, coagulation and axial convection of particles can exceed the effect of particle diffusion in the region and this leads to similar distributions irrespectively of considering particle diffusion (see Figs. 3(a) and (b)). At $x = 0.5$ mm, the difference between cases with or without particle diffusion is noticeable; the case without particle diffusion yields very small amount of very small particles with D_s close to two while the case considering diffusion shows relatively large amount of small particles with D_s ranging widely from two to three. These small particles are originated from upper regions where chemical reactions are active since there should be little particle formation near $x = 0.5$ mm as evidenced from Fig. 4. Similarly, the size distributions near the particle stagnation point are much

different since particle axial velocities are small in the region and small particles generated in the upstream region can diffuse up to the particle stagnation point.

The effect of particle diffusion can be more easily seen in comparisons of volume equivalent size distributions as depicted in Fig. 5. The size distributions at $x = 0.5$ and 5.5 mm are significantly different while the size distributions at $x = 3.5$ mm are similar. At $x = 5.5$ mm, large difference between these two cases for small particle diameters results from the diffusion of small particles. It is interesting to note that both distributions at $x = 5.5$ mm are bi-modal irrespectively of including particle diffusion. This suggests that the nature of bi-modal distribution comes from the competition between particle generation and coagulation and the effect of axial diffusion would only intensify this bi-modality. The reason why bi-modal distributions were obtained at $x = 5.5$ mm where particle generations no longer took place would be simply due to the convection of bi-modal sizes occurred in the upstream zone where chemical reactions were active.

3.3. Testing of different coalescence models

As mentioned earlier, there would be no established theory on the coalescence characteristic time for very small primary particles less than about 10 nm in diameter. Therefore, in the present study, several different sintering or coalescence models have been used and compared one another and also with the existing experimental data. The size distributions in two-dimensional particle space have been obtained for four different sintering models; viscous flow sintering, fast sintering for small particles up to particles composed of 1024 monomers and viscous flow sintering for larger particles (Ulrich & Subramanian, 1977; Windeler et al., 1997), atomistic diffusion mechanism (Ehrman, 1999) and hybrid model combining atomistic diffusion and viscous flow sintering. For the fast sintering model, sphere particles are assumed for first 10 sections and non-spherical particles are considered for the rest of sections. Therefore, for the first 10 sections, $V_k (= \int_{v_{k-1}}^{v_k} vn^*(v)\,\mathrm{d}v)$ is solved instead of $V_{k,l}$. For the hybrid model, it is attempted to choose the smaller characteristic time for coalescence from atomistic diffusion and viscous flow sintering models. Therefore, atomistic diffusion mechanism is used for small particles and viscous flow sintering model for large particles (the boundary size depends on temperature, for example, the size was about 8 nm at $T = 2000$ K). Atomistic diffusion mechanism would be valid only for small particles and can result in large error for large particles in which viscous flow sintering model is more appropriate and would result in good agreement with experimental data (Seto et al., 1997). Comparing with the results obtained from viscous flow sintering model (case (a)) in Fig. 6), it is clearly shown that the use of atomistic diffusion model for all particle size (case (b) in Fig. 6) results in enhanced coalescence for small particles but retarded coalescence for large particles. However, the use of hybrid model (case (c) in Fig. 6) shows the overall enhancement of sintering for all particle sizes. It is noted that the hybrid model yields the similar profile of size distribution to atomistic diffusion model for small particle size and for large particle size, the distributions are similar to the results obtained from viscous flow sintering model.

Variations of primary particle growth were also examined for different sintering models (shown in Fig. 7(a)). Mean diameter of primary particles was evaluated as $6V_t/A_t$ where V_t is the total volume concentration and A_t is the total area concentration. Primary particle sizes estimated from atomistic diffusion coalescence model were larger until $x = 4.4$ mm where the size was about 0.01 μm (10 nm), and has become smaller beyond $x = 4.4$ mm. The characteristic coalescence time

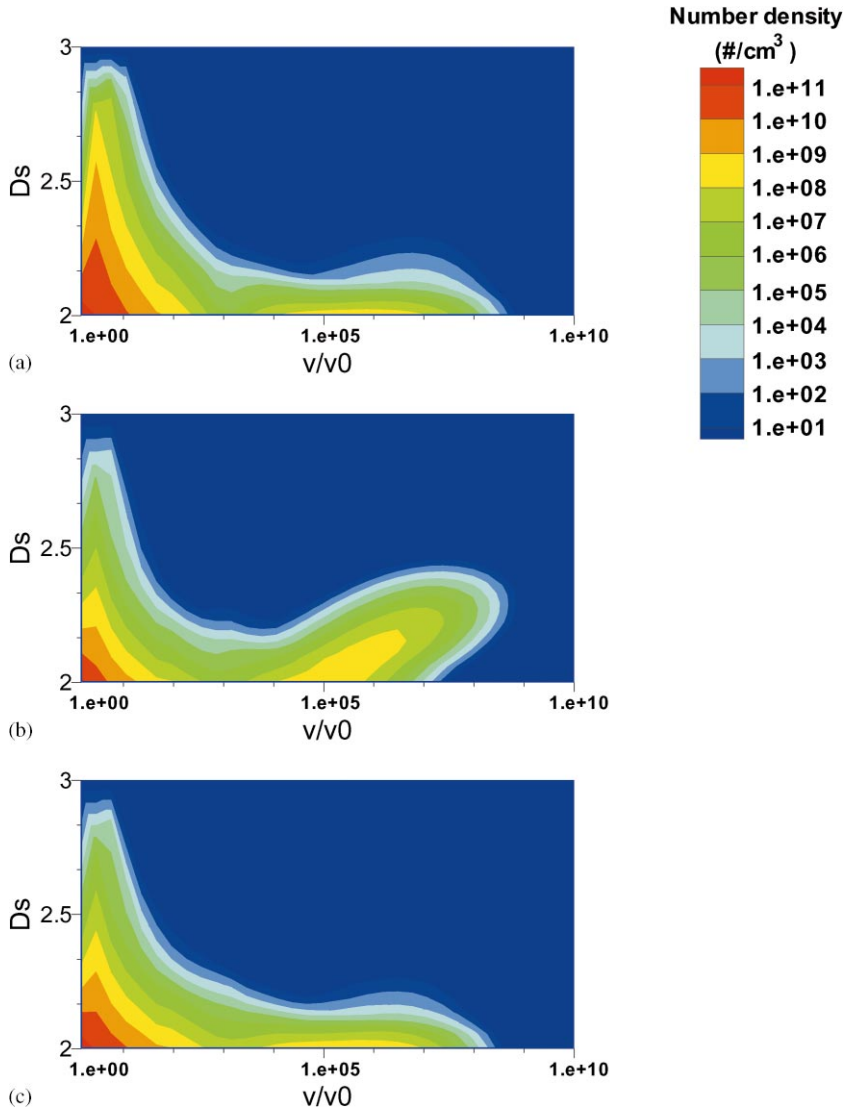

Fig. 6. Comparisons of size distributions in two-dimensional particle space at $x = 5.5$ mm for different sintering models: (a) viscous flow sintering model, (b) atomistic diffusion sintering model and (c) hybrid model (atomistic + viscous).

for the atomistic diffusion mechanism (Eq. (14)) becomes larger than that for the viscous flow mechanism (Eq. (13)) for particles larger than 5 nm in diameter at $T = 2122$ K (at $x = 4.4$ mm). Since the viscous flow sintering model has been shown to agree with experimental data for large particles (Seto et al., 1997), it should be more reasonable to use viscous flow sintering model for large particles. This leads, in the present study, the use of hybrid model that utilizes faster coalescence rate between atomistic diffusion and viscous flow mechanisms. Fig. 7(a) shows that the hybrid model first follows the growth line of the atomistic diffusion mechanism until $x = 4.4$ mm

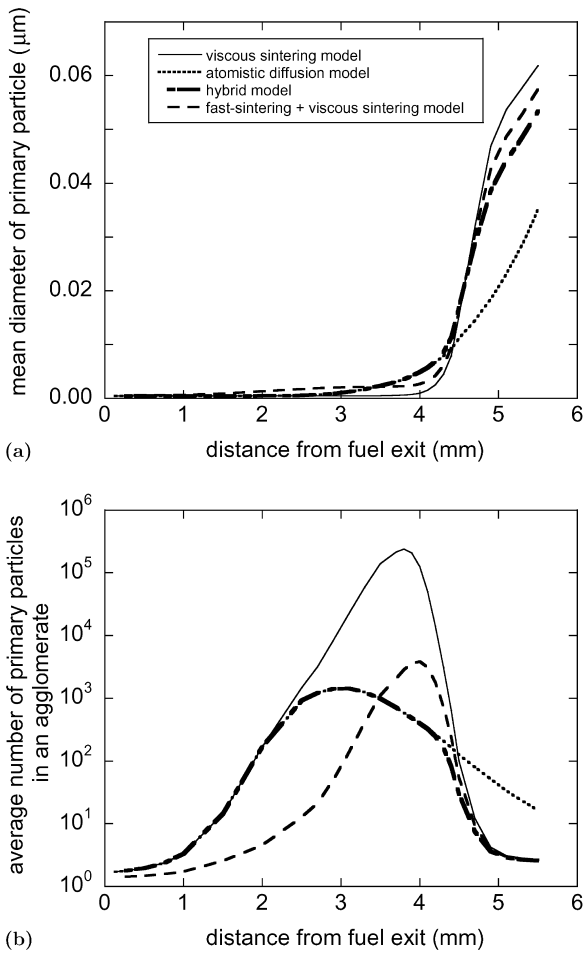

Fig. 7. Variations of (a) primary particle diameter and (b) average number of primary particles in an agglomerate when using four different sintering models; viscous flow, atomistic diffusion, fast sinterig and hybrid models.

and then deviates from the dotted line (atomistic diffusion model) and tends to approach closely to the viscous flow sintering case. Note that viscous flow sintering model finally resulted in the largest size near particle stagnation point due to the combined effect of sintering and coagulation of particle. Enhanced sintering when using the atomistic diffusion or hybrid model could make more spherical-like particles that should have less collision cross sections than non-spherical particles, which can lead smaller particles. Therefore, the information about the variation of primary particle size could not be sufficient to represent the extent of sintering. Average number of primary particles in an agglomerate was shown in Fig. 7(b). As shown in Fig. 7(b), the average number of primary particles is smallest when using the hybrid model even though the viscous flow sintering model results in the largest primary particle size (Fig. 7(a)). As suggested by Ulrich and Subramanian (1977) and Windeler et al. (1997), it is assumed for fast sintering model that particles having less than 1024 monomers coalesce instantaneously to form spherical particles and larger particles sinter

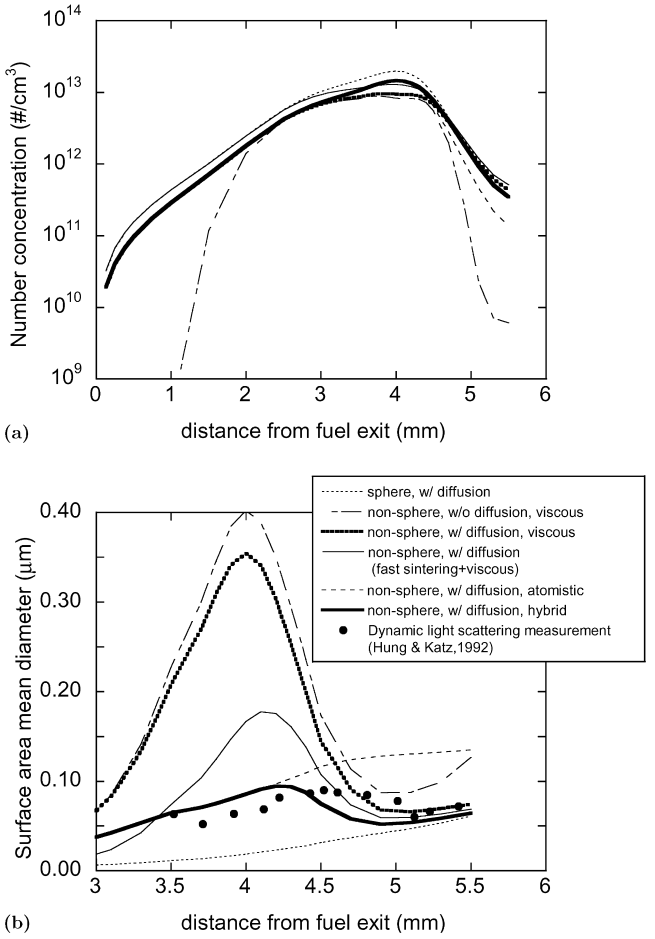

Fig. 8. Variations of (a) total number concentrations and (b) surface area mean diameters for four different sintering models of non-spherical particle growth with or without Brownian particle diffusion. The comparisons of the variation of surface area mean diameters between the calculations and the existing experimental data were also made.

following the viscous sintering model. Fast sintering model also shows the significant enhancement of sintering as shown in Fig. 7(b)

Fig. 8 shows the variations of total number concentration and surface area mean diameter for different sintering models with or without particle diffusion. The variations of number density are similar except the case that does not consider particle diffusion. Initial increase of total number concentration and later decrease are due to particle generation caused by chemical reactions and particle coagulation, respectively. Note that the significantly higher number densities both near the burner exit and the stagnation point should be the results of particle diffusion. Fig. 8(b) shows that the sphere model predicts the smallest particle size. The smaller sizes for sphere model were resulted by less collision cross sections for spheres than their volume equivalent non-spherical particles.

Sphere model obviously predicts the monotonic increase of particle size. On the other hand, non-spherical models show the increase of diameters at the initial stage and then the decrease of diameters at the later stage due to the effect of coalescence, which is consistent with Hung and Katz (1992). For non-spherical models, the use of the hybrid model was shown to yield the smallest sizes while viscous flow sintering model resulted in the largest. In Fig. 8(b), measurement data obtained by dynamic light scattering (Hung & Katz, 1992) were also included. It is not clear which average diameter from the simulation should be compared with the mobility equivalent diameters measured by dynamic light scattering. Considering that Brownian diffusion coefficient is related to the surface area in free molecular regime and dynamic light scattering measurement is known to have poor sensitivity for small particles although no size limit in principle and therefore, the measurement would be heavily weighted toward large particles (Zachariah et al., 1989), surface area mean diameters of the present simulation were compared with experimental data. In the present study, the hybrid model resulted in the best agreement with data.

4. Conclusions

The evolution of the size distribution for non-spherical particle growth undergoing generation, convection, diffusion, coagulation and coalescence has been studied in a counterflow diffusion flame solving a two-dimensional aerosol dynamics. Flame analysis of multi-step chemical reactions of hydrogen/oxygen including both oxidation and hydrolysis of $SiCl_4$ has been preceded and the variations of flame temperature, concentration of different gas species and particle generations were obtained. Predicted flame temperatures were compared with the existing experimental data and were in good agreement. Comparing to particle growth model assuming spherical particles, non-spherical particle growth model adopted in the present simulation resulted in significantly larger sizes due to the enhanced coagulation of non-spherical particles with larger collision cross sections. The effect of the axial particle diffusion was also investigated and found to be significant to alter the size distributions especially near the burner exit and the stagnation plane in a counterflow diffusion flame. Bi-modal size distributions were obtained because of the existence of both mechanisms of chemical reactions and coagulation. Analysis of a two-dimensional aerosol dynamics correctly predicted the evolution of non-spherical particle growth showing the competing effect of collision and coalescence of particles. As a result, surface area mean diameters increase at the initial stage due to the effect of coagulation and then decrease at the later stage due to the effect of coalescence. Four different sintering models were examined including viscous flow sintering, fast sintering, atomistic diffusion and hybrid models. Enhanced sintering models obviously resulted in smaller size due to the effect of reducing collision cross sections for enhanced sintered particles. The hybrid model utilizing atomistic diffusion sintering for small particles and viscous flow sintering for large particles yielded the best agreement with the existing experimental data.

Acknowledgements

This work was funded by Creative Research Initiatives program of Korean Ministry of Science and Technology (Center for Nano Particle Control).

References

Allendorf, M. D., Bautista, J. R., & Potkay, E. (1989). Temperature measurements in a vapor axial deposition flame by spontaneous Raman spectroscopy. *Journal of Applied Physics*, *66*, 5046–5051.

Chang, H., & Biswas, P. (1992). In situ light scattering dissymmetry measurements of the evolution of the aerosol size distribution in flames. *Journal of Colloid and Interface Science*, *153*, 157–166.

Cho, J., Kim, J., & Choi, M. (1998). An experimental study of heat transfer and particle deposition during the outside vapor deposition process. *International Journal of Heat and Mass Transfer*, *41*, 435–445.

Chung, S. L., & Katz, J. L. (1985). The counterflow diffusion flame burner: A new tool for the sturdy of the nucleation of refractory compounds. *Combustion and Flame*, *61*, 271–284.

Chung, S. L., Tsai, M. S., & Lin, H. D. (1991). Formation of particles in a H_2–O_2 counterflow diffusion flame doped with SiH_4 or $SiCl_4$. *Combustion and Flame*, *85*, 134–142.

Ehrman, S. H. (1999). Effect of particle size on rate of coalescence of silica nanoparticles. *Journal of Colloid and Interface Science*, *213*, 258–261.

Ehrman, S. H., Friedlander, S. K., & Zachariah, M. R. (1998). Characteristics of SiO_2/TiO_2 nanocomposite particles formed in a premixed flat flame. *Journal of Aerosol Science*, *29*, 687–706.

Friedlander, S. K. (1977). *Smoke, dust and haze*. New York: Wiley.

Gelbard, F., Tambour, Y., & Seinfeld, J. H. (1980). Sectional representations for simulating aerosol dynamics. *Journal of Colloid and Interface Science*, *76*, 541–556.

Hung, C. H., & Katz, J. L. (1992). Formation of mixed oxide powders in flames: Part I. TiO_2–SiO_2. *Journal of Materials Research*, *7*, 1861–1869.

Kim, K. S., & Pratsinis, S. E. (1988). Manufacture of optial waveguide preforms by modified chemical vapor deposition. *A.I.Ch.E. Journal*, *34*, 912–921.

Koch, W., & Friedlander, S. K. (1990). The effect of particle coalescence on the surface area of a coagulation aerosol. *Journal of Colloid and Interface Science*, *140*, 419–427.

Kochubei, V. F. (1997). Kinetics of the gas-phase hydrolysis of silicon tetrachloride. *Kinetics and Catalysis*, *38*, 212–214.

Kruis, F. E., Kusters, K. A., Pratsinis, S. E., & Scarlett, B. (1993). A simple model for the evolution of the characteristics of aggregate particles undergoing coagulation and sintering. *Aerosol Science and Technology*, *19*, 514–526.

Maas, U., & Warnatz, J. (1988). Ignition processes in hydrogen–oxygen mixtures. *Combustion and Flame*, *74*, 53–69.

Mandelbrot, B. B. (1983). *The fractal geometry of nature*. New York: Freeman and Company.

Nazaroff, W. W., & Cass, G. R. (1987). Particle deposiotion from a natural convection flow onto a vertical isothermal flat. *Journal of Aerosol Science*, *18*, 445–455.

Okuyama, K., Shimada, M., Fujimoto, T., Maekawa, T., Nakaso, K., & Seto, T. (1998). Effects of preparation conditions on the characteristics of titanium dioxide particles produced by a CVD method. *Journal of Aerosol Science*, *29*, S907–S908.

Powers, D. R. (1978). Kinetics of $SiCl_4$ oxidation. *Journal of the American Ceramic Society*, *61*, 295–297.

Pratsinis, S. E. (1998). Flame aerosol synthesis of ceramic powders. *Progress in Energy and Combustion Science*, *24*, 197–219.

Rogak, S. N., & Flagan, R. C. (1992). Coagulation of aerosol agglomerates in the transition regime. *Journal of Colloid and Interface Science*, *151*, 203–224.

Seto, T., Shimada, M., & Okuyama, K. (1995). Evaluation of sintering of nanometer-sized Titania using aerosol method. *Aerosol Science and Technology*, *23*, 183–200.

Seto, T., Hirota, A., Fujimoto, T., Shimada, M., & Okuyama, K. (1997). Sintering of polydisperse nanometer-sized agglomerates. *Aerosol Science and Technology*, *27*, 422–438.

Smooke, M.D., Puri, I.K., & Seshadri, K. (1986). A comparison between numerical calculations and experimental measurements of the structure of a counterflow diffusion flame burning diluted methane in diluted air. *Proceedings of 21st (international) symposium on combustion*, (pp. 1783–1792).

Talbot, L., Cheng, R. K., Schefer, R. W., & Willis, D. R. (1980). Thermophoresis of particles in a heated boundary layer. *Journal of Fluid Mechanics*, *101*, 737–758.

Ulrich, G. D., & Subramanian, N. S. (1977). Particle growth in flames III. Coalescence as a rate-controlling process. *Combustion Science and Technology*, *17*, 119–126.

Windeler, R. S., Lehtinen, K. E. J., & Friedlander, S. K. (1997). Production of nanometer-sized metal oxide particles by gas reaction in a free jet. II: Particle size and neck formation-comparison with theory. *Aerosol Science and Technology*, *27*, 191–205.

Wooldridge, M. S. (1998). Gas-phase combustion synthesis of particles. *Progress in Energy and Combustion Science*, *24*, 63–87.

Xiong, Y., Pratsinis, S. E., & Weimer, A. W. (1992). Modeling the formation of boron-carbide particles in an aerosol flow reactor. *A.I.Ch.E. Journal*, *38*, 1685–1692.

Xiong, Y., & Pratsinis, S. E. (1993). Formation of agglomerate particles by coagulation and sintering — Part I. A two dimensional solution of the population balance equation. *Journal of Aerosol Science*, *24*, 283–300.

Zachariah, M. R., Chin, D., Semerjian, H. G., & Katz, J. L. (1989). Dynamic light scattering and angular dissymmetry for the in-situ measurement of silicon dioxide particle synthesis in flames. *Applied Optics*, *28*, 530–536.

Zachariah, M. R., & Semerjian, H. G. (1989). Simulation of ceramic particle formation: Comparison with in-situ measurements. *A.I.Ch.E. Journal*, *35*, 2003–2012.